

# Field Experience With an Ultra-High-Speed Line Relay and Traveling-Wave Fault Locator

Sthitaprajnya Sharma and Mangapathirao V. Mynam  
*Schweitzer Engineering Laboratories, Inc.*

Presented at the  
45th Annual Western Protective Relay Conference  
Spokane, Washington  
October 16–18, 2018

# Field Experience With an Ultra-High-Speed Line Relay and Traveling-Wave Fault Locator

Sthitaprajnay Sharma and Mangapathirao V. Mynam, *Schweitzer Engineering Laboratories, Inc.*

**Abstract**—This paper shares an Indian utility’s field experience with ultra-high-speed (UHS) protection and traveling-wave fault locating (TWFL). One of India’s major utilities was looking to reduce the time and effort it takes to locate faults on their 110 kV, 57.4 km transmission line. This line includes a tap and passes through difficult terrain (including forests and river and railway crossings), which contributes to challenges in locating faults. The utility installed UHS line protective relays with TWFL capability to accurately locate faults. This paper discusses the application of these relays and presents the performance of both protection and fault locating functions for internal faults on the line. We also analyze one of the events captured at 1 MHz that includes a circuit breaker restrike. The events also show incipient faults that evolved to faults detectable by conventional line relays.

## I. INTRODUCTION

Accurate fault location is critical to power system utility operations. Indian utilities are looking to apply traveling-wave fault locators to accurately locate faults on their transmission networks. One of these utilities installed line protective relays with ultra-high-speed (UHS) protection elements and traveling-wave fault locating (TWFL) functionality on a 110 kV, 57.4 km line. The 110 kV transmission line traverses hills and forests and has a river crossing and a line tap. This line challenged existing impedance-based fault locating methods and caused difficulties for the patrol teams locating the faults.

Additionally, major utilities and regulators are paying attention to the System Average Interruption Frequency Index (SAIFI) and System Average Interruption Duration Index (SAIDI) performance indicators. Accurate fault locating and fast clearing drive these indices. Locating temporary faults and addressing their causes (e.g., replacing a damaged insulator) avoids recurring faults, which improves these indices.

TWFL methods provide accurate fault location [1]. This technology has been available in standalone fault locators for decades [2]; however, utilities applied these dedicated standalone fault locators almost exclusively on extra-high-voltage power lines. Now, line protective relays with TWFL capability are available, which has led utilities to use this proven technology on subtransmission lines as well.

This paper discusses the pilot installation of line protective relays with TWFL and UHS protection functions on the utility’s pilot 110 kV line. We first summarize the TWFL and UHS protection principles [3] [4] [5]. Then, we discuss the performance of these fault locating and protection functions for three internal faults. In particular, we analyze one of the events where the line protective relays captured a circuit breaker restrike. We also show event records that captured incipient faults, which evolved into faults detectable by conventional line

relays. We think that these incipient faults are due to insulation degradation causing temporary arcing. It is exciting to have devices that record such events; this capability provides researchers with data that can be used to develop and improve algorithms to detect and locate incipient faults.

## II. OVERVIEW OF TWFL AND UHS PROTECTION PRINCIPLES

In this section, we briefly discuss the fault locating methods and UHS protection principles available in the installed line protective relay for the pilot installation.

### A. Fault Locating

Faults on transmission lines generate traveling waves that propagate from the location of the fault to the line terminals. The fault location can be calculated based on the wave arrival times, the line length, and the traveling-wave line propagation time. TWFL provides better accuracy than impedance-based fault locating methods. For example, on a 100 km line, TWFL provides accuracy of approximately 300 meters compared to the approximately 1 km accuracy of a double-end impedance-based fault locating method or the 1 to 5 km (or poorer) accuracy of a single-end impedance-based method. The line protective relay used in this application includes single-end and double-end fault locating functions using traveling-wave-based and impedance-based methods.

The double-end TWFL method uses the first wave arrival times from both terminals, along with the line length and the traveling-wave line propagation time, to calculate the fault location. The exchange of the wave arrival time information can be achieved by various means. Exchanging information using a direct fiber-optic connection between the two relays (one at each terminal) is one option. Another option is for each relay to send the wave arrival times to a central system. This system uses the wave arrival times and the line parameters to compute the fault location. Equation (1) shows the double-end method fault location calculation.

$$\text{TWFL}_{\text{DE}} = \frac{\text{LL}}{2} \cdot \left( 1 + \frac{t_A - t_B}{\text{TWLPT}} \right) \quad (1)$$

where:

$\text{TWFL}_{\text{DE}}$  is the fault location using the double-end traveling-wave-based method.

LL is the line length.

$t_A$  is the first traveling-wave arrival time at Terminal A.

$t_B$  is the first traveling-wave arrival time at Terminal B.

TWLPT is the traveling-wave line propagation time.

The single-end TWFL method uses the first wave arrival time, the arrival time of the first wave reflected from the fault, and the line propagation time and length to compute the fault location. Equation (2) shows the single-end method fault location calculation.

$$\text{TWFL}_{\text{SE}} = \frac{\text{LL}}{2} \cdot \left( \frac{\text{t}_{\text{A\_REFLECTION}} - \text{t}_{\text{A}}}{\text{TWLPT}} \right) \quad (2)$$

where:

$\text{TWFL}_{\text{SE}}$  is the fault location using the single-end traveling-wave-based method.

LL is the line length.

$t_{\text{A}}$  is the first traveling-wave arrival time at Terminal A.

$t_{\text{A\_REFLECTION}}$  is the arrival time at Terminal A of the first wave reflected from the fault.

### B. UHS Protection Elements

The line protective relay used in this installation includes a Zone 1 underreaching incremental-quantity distance element (TD21), a permissive overreaching transfer trip (POTT) scheme with a traveling-wave directional element (TW32) and an incremental-quantity directional element (TD32), and a traveling-wave current differential scheme (TW87) over a direct fiber-optic channel.

#### 1) Incremental-Quantity Distance Element, TD21

The distance element principle is based on the fact that the incremental voltage at the fault location cannot be higher than the pre-fault voltage at the fault location. The TD21 element operates if the calculated voltage change (the operating voltage,  $V_{21OP}$ ) at the reach point exceeds the pre-fault voltage at the reach point (the restraining voltage,  $V_{21RST}$ ). Reference [5] derives the theory of the TD21 element.

#### 2) Traveling-Wave Directional Element, TW32

The traveling-wave directional element uses phase voltage and current traveling waves [5]. The element calculates the torque as a product of the current traveling wave and the sign-inverted voltage traveling wave. TW32 declares forward if the integrated torque is positive and declares reverse if the integrated torque is negative. This element is used as part of the POTT protection scheme.

#### 3) Incremental-Quantity Directional Element, TD32

The TD32 element is realized using instantaneous incremental quantities. Reference [5] provides the theory behind the incremental quantities. Similar to the TW32 element, the TD32 element calculates the operating torque (TOP) as the product of the instantaneous sign-inverted incremental voltage and the incremental replica current. TD32 calculates the forward restraining torque (TFWD) and the reverse restraining torque (TREV) as the product of the square of the replica current and the respective forward and reverse impedance thresholds. The TD32 element integrates the torques (TOP, TFWD, and TREV) and compares the integrated operating torque with the integrated restraining torques. The TD32 element declares forward if the integrated operating torque TOP exceeds the integrated forward restraining torque TFWD, and it declares reverse if the integrated operating torque

TOP is less than the integrated reverse restraining torque –TREV. TD32 is used as part of the POTT protection scheme.

#### 4) Traveling-Wave Current Differential Scheme, TW87

The TW87 scheme compares the timing, polarities, and magnitudes of the current traveling waves at both line terminals [5]. The line relays at each end exchange data sampled at 1 MHz using a direct fiber-optic connection. For external events, the current traveling wave enters at one line terminal, and after the line propagation time, the wave leaves the other terminal with the opposite polarity. For internal faults, the polarities of the local and remote current traveling waves are the same, and the first waves from the two terminals are spaced, in time, less than the line propagation time.

Reference [6] shows that the operating times for UHS protection elements are on the order of 2 ms for the TD32 element, less than 1 ms for the TW32 element, 4 ms for the TD21 element, and less than 1 ms plus the channel time for the TW87 scheme.

### III. COMMISSIONING AND MEASURING LINE PROPAGATION TIME

The 110 kV transmission line traverses inaccessible terrain and has a tap 22.8 km from Terminal R and 34.6 km from Terminal L. Fig. 1 shows the system one-line diagram.

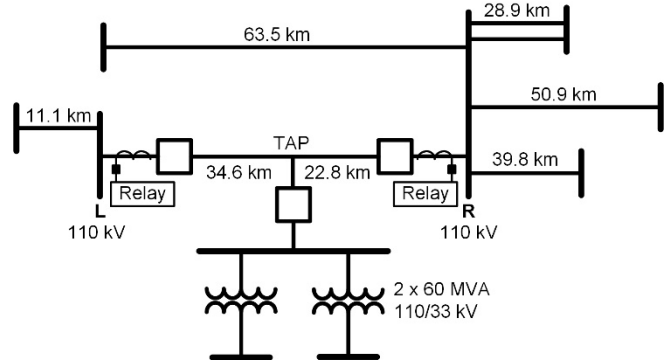


Fig. 1. Utility 110 kV system showing the pilot line between Terminals L and R

The utility installed line relays with TWFL functionality at each end of the 110 kV transmission line. They wired the relays in series with the in-service protective relays at both ends. In this system, Terminal L has a 1 A nominal current transformer (CT), and Terminal R has a 5 A CT.

Table I lists the line and relay parameters.

TABLE I  
PILOT LINE PARAMETERS

<b>Line Length</b>	57.4 km
<b>Positive-Sequence Impedance</b>	$15.0 \angle 74.76^\circ \Omega$ primary
<b>Zero-Sequence Impedance</b>	$60.525 \angle 80.02^\circ \Omega$ primary
<b>CT Ratio (Terminal L)</b>	1200/1
<b>VT Ratio (Terminal L)</b>	110000/110
<b>CT Ratio (Terminal R)</b>	600/5
<b>VT Ratio (Terminal R)</b>	110000/110

The TD21 phase and ground distance elements were set to 70 percent and 65 percent of the line impedance at Terminals L and R, respectively. The stations have end-to-end direct fiber-optic communications channels. The channel losses were high, preventing use of the point-to-point channel for the POTT and TW87 schemes. The relays were synchronized to absolute time using satellite (Global Positioning System [GPS]) clocks for convenient event analysis and offline double-end TWFL.

An accurate line propagation time value is required for fault location accuracy. As recommended in [7], an energization of the 110 kV transmission line was planned to determine the line propagation time. During pole closing, a step change in voltage is applied to the line at the closing end. This step change propagates to the remote terminal, reflects from the open terminal, and arrives back at the closing terminal. The line energization test was performed from Terminal L with the line open at Terminal R, and then vice versa, to determine the line propagation time. The relays captured event records during the line energization. Fig. 2 shows the voltages and currents captured during the line energization from Terminal R.

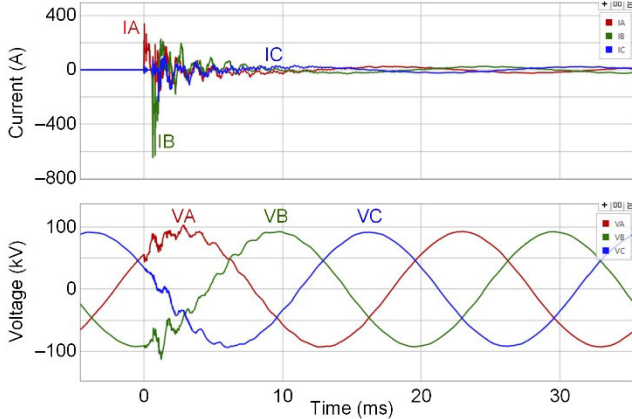


Fig. 2. Phase currents and voltages captured during the line energization test from Terminal R

Fig. 3 shows the current traveling waves obtained by filtering (using a differentiator smoother [5]) the 1 MHz sampled signals shown in Fig. 2. Note that the wave reflection from TAP was received prior to the reflection from the open Terminal L. The line propagation time was calculated as one-half of the time difference between the pole closure and the arrival of the reflected wave from the open terminal. The line propagation time value was 199.075  $\mu$ s.

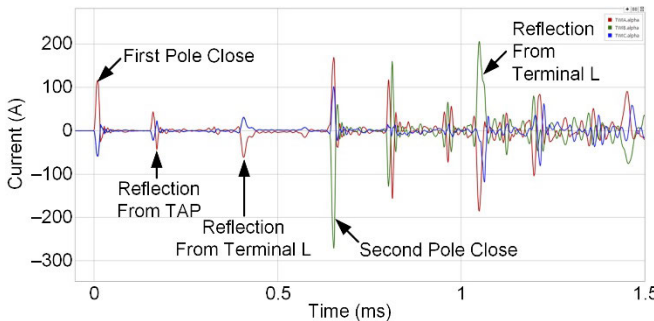


Fig. 3. Current traveling waves captured during the line energization test at Terminal R

#### IV. PERFORMANCE OF THE FAULT LOCATOR AND PROTECTION ELEMENTS

Over a one-week period, the line relays recorded three internal faults. In this section, we analyze these events and evaluate the performance of the fault locating and protection functions. Due to the lack of relay-to-relay communication during these events, we show the performance of the directional elements instead of that of the POTT scheme. We used event records from both line terminals with relays synchronized to GPS to calculate the fault location using the double-end TWFL method.

##### A. Phase-A-to-Ground Fault, January 17, 2018

###### 1) Performance of UHS Protection Elements

Fig. 4 shows the voltages and currents captured at Terminal L during the first fault. The incremental-quantity directional element (TD32) and distance element (TD21) operated in 2 ms and 10 ms, respectively.

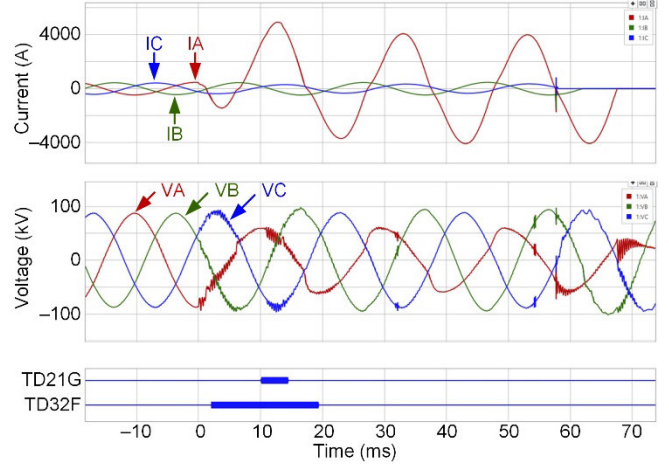


Fig. 4. Currents and voltages captured at Terminal L for the January 17, 2018 fault

This fault was at 42 percent of the Zone 1 distance element reach. As expected, the distance element operated. Fig. 5 shows the fault loop operating voltage (VFAG) exceeding the restraining voltage (VRAG).

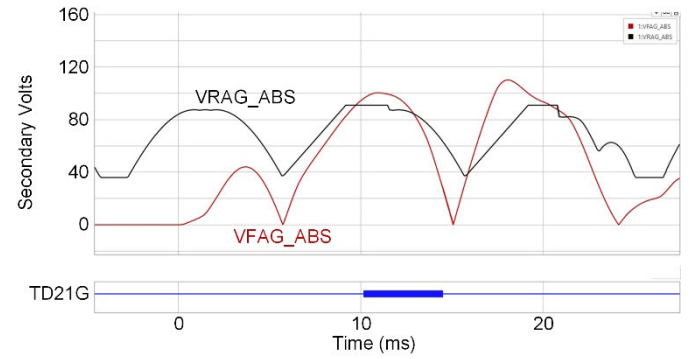


Fig. 5. Ground distance element operation for the January 17, 2018 fault at 42 percent of the reach setting

Fig. 6 shows the incremental loop voltage and replica current for this fault. For a forward event, these signals are

opposite in sign, and the ratio of their magnitudes is equal to the source impedance magnitude. The source impedance was calculated based on the incremental voltage and the incremental replica current, and the source impedance was equal to  $4.3 \Omega$  secondary. As expected, the TD32 element operated for this forward event. Fig. 7 shows the operating torque, the forward and restraining torques, and the operation of the TD32 element. The element declares a forward event when the integrated operating torque exceeds the integrated forward restraining torque.

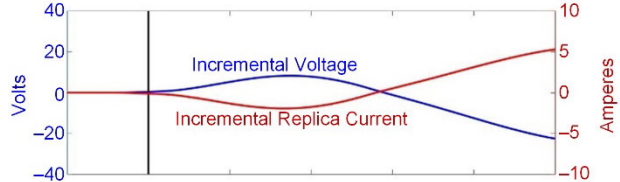


Fig. 6. Phase A incremental loop voltage and replica current at Terminal L for the January 17, 2018 fault

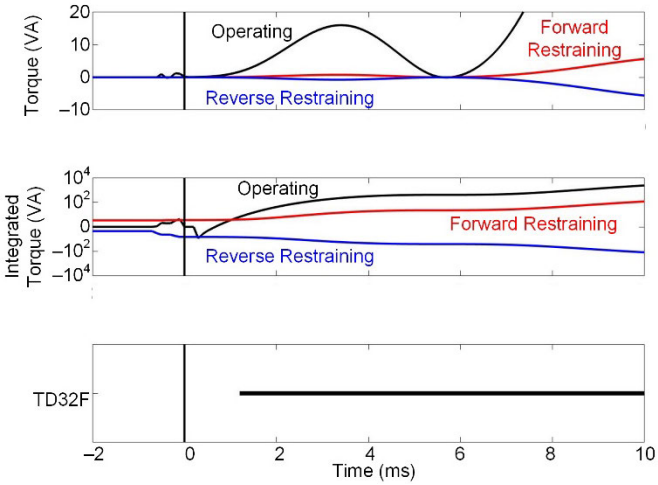


Fig. 7. Phase A TD32 element torques and integrated torques at Terminal L for the January 17, 2018 fault

At Terminal R, the incremental-quantity and traveling-wave directional elements operated in less than 3 ms. From Terminal R, the fault was at 100 percent of the Zone 1 distance element reach setting. Fig. 8 shows the voltages and currents captured at Terminal R.

Fig. 9 shows the operating and restraining voltages for this fault at 100 percent of the reach setting from Terminal R. Since the operating voltage was less than the restraining voltage, the TD21 element did not operate. The operating voltage was considerably lower than the restraining voltage even though the

fault was near the reach point. This is because the fault was resistive.

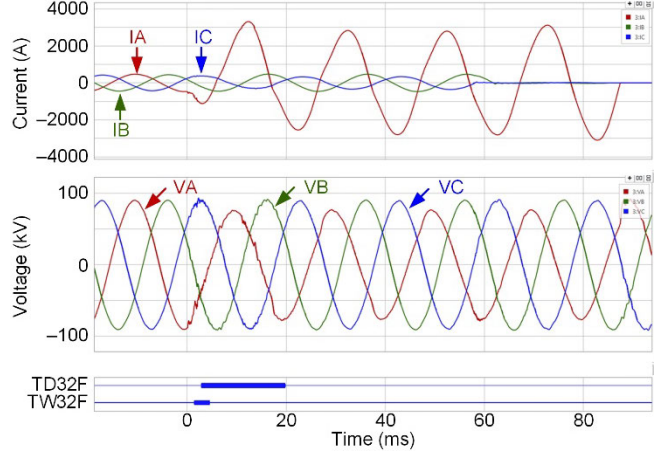


Fig. 8. Currents and voltages captured at Terminal R for the January 17, 2018 fault

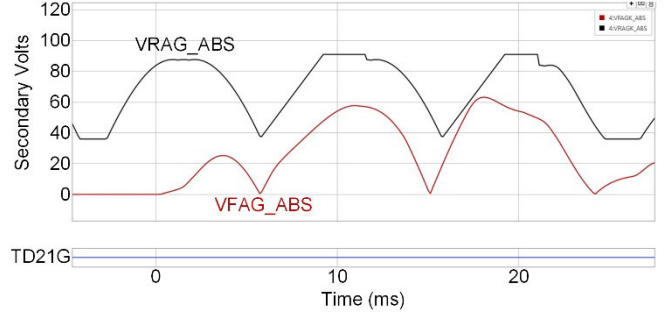


Fig. 9. TD21 did not operate for the January 17, 2018 fault at 100 percent of the reach

## 2) Fault Location and Circuit Breaker Operation

Fig. 10 shows the traveling-wave currents (alpha mode) from Terminals L and R associated with Phase A. Analysis of the current traveling waves showed that there was an incipient fault 1 ms prior to the Phase-A-to-ground fault in the same location. Based on the first wave arrival times, the fault locations calculated for the two events (the incipient fault and the fault) from Terminal L are as shown in (3) and (4), respectively.

$$FL1_L = \frac{57.4 \text{ km}}{2} \cdot \left( 1 + \frac{-83.06 \mu\text{s}}{199.075 \mu\text{s}} \right) = 16.73 \text{ km} \quad (3)$$

$$FL2_L = \frac{57.4 \text{ km}}{2} \cdot \left( 1 + \frac{-82.22 \mu\text{s}}{199.075 \mu\text{s}} \right) = 16.85 \text{ km} \quad (4)$$

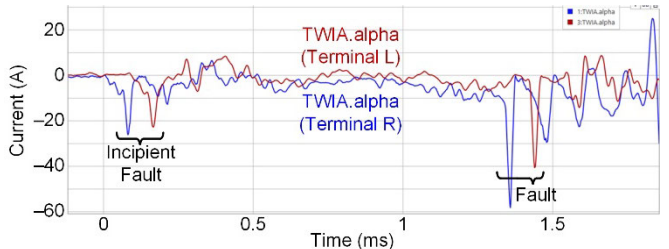


Fig. 10. Phase A current traveling waves from Terminals L and R for the January 17, 2018 fault

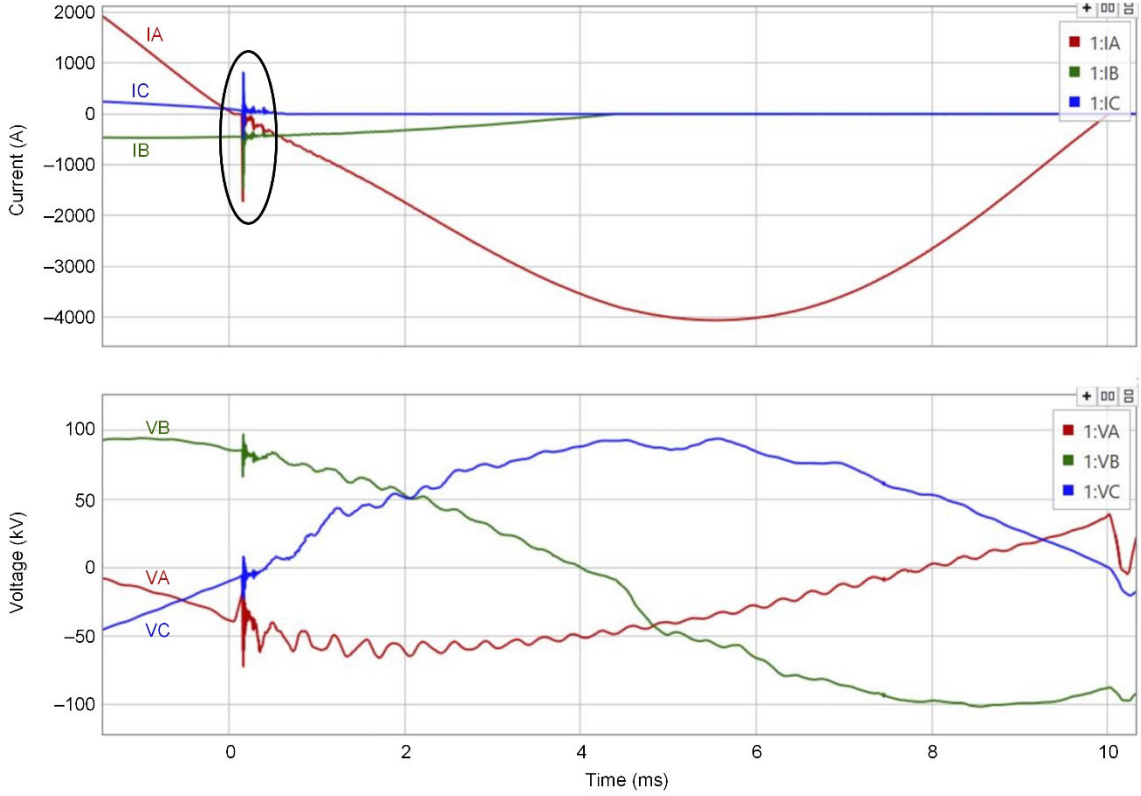


Fig. 11. Currents and voltages captured during a circuit breaker restrike at Terminal L for the January 17, 2018 fault

The TWFL-enabled relay also recorded a circuit breaker restrike when the breaker opened at Terminal L. Fig. 11 shows a significant change in current (indicated with a circle) after the current zero crossing when the circuit breaker was supposed to clear the fault. The fault lasted half a cycle longer because of the circuit breaker restrike.

Megahertz-sampled data proved beneficial to identifying potential issues in the primary equipment. In this case, the recorded data provided insight into the circuit breaker operation.

#### B. Phase-A-to-Ground Fault, January 18, 2018

Fig. 12 shows the voltages and currents captured at Terminal L for the second fault. The traveling-wave directional element (TW32) operated in 110  $\mu$ s, and the incremental-quantity directional element (TD32) operated in 1.31 ms. Fig. 13 shows the voltages and currents captured at Terminal R. The directional elements operated in less than 1.24 ms and the

distance element (TD21) operated in 2.54 ms. This fault was at 40 percent of the Zone 1 reach setting from Terminal R.

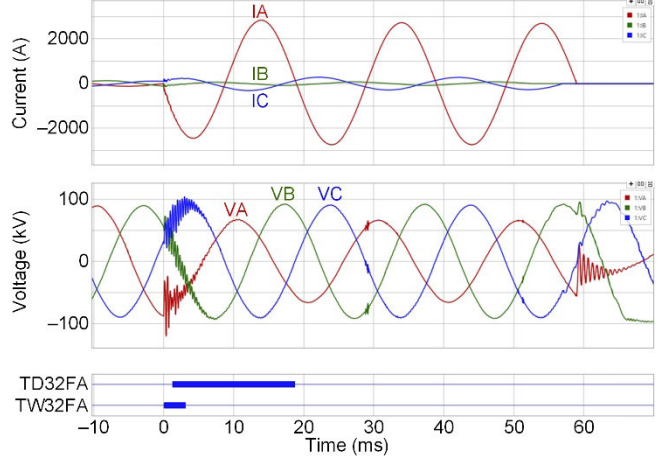


Fig. 12. Currents and voltages captured at Terminal L for the January 18, 2018 fault

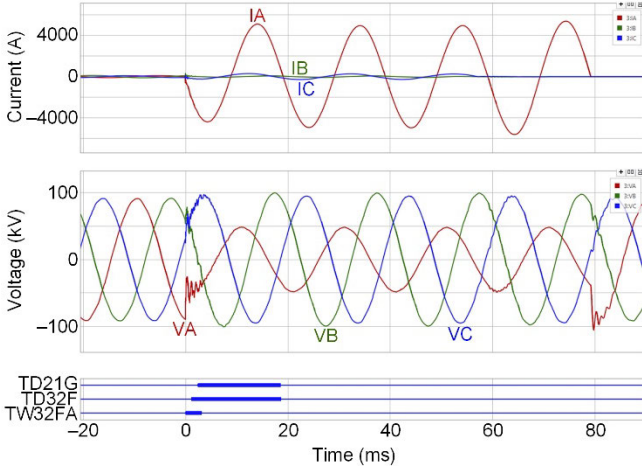


Fig. 13. Currents and voltages captured at Terminal R for the January 18, 2018 fault

Fig. 14 shows the current and voltage traveling waves associated with this fault. It shows how the CT and capacitively coupled voltage transformer (CCVT) responded for the first wave. CTs provide faithful reproductions of the actual traveling wave shapes. CCVTs rely on stray capacitances to provide high-frequency signals to the relay inputs. This voltage traveling-wave measurement is not accurate in terms of voltage traveling-wave magnitude, but it is accurate in terms of polarity for a few tens of microseconds [8]. To account for this CCVT behavior, the TW32 element only uses the first wave information from both the current and the voltage traveling waves. As explained in Section II, the TW32 element declares a forward event if the integrated torque during the initial few tens of microseconds exceeds a threshold. In this event, the TW32 element operated in less than 50  $\mu$ s at Terminal R.

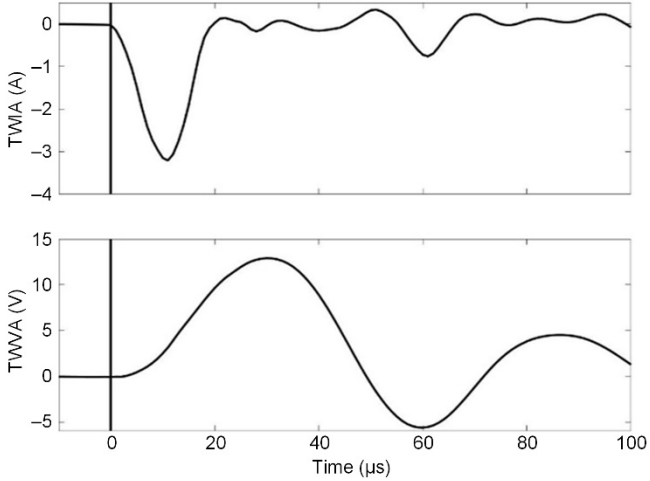


Fig. 14. Traveling wave phase current and voltage are of opposite polarity for the forward event

Fig. 15 shows the torque (the traveling-wave current multiplied by the negative traveling-wave voltage) and the integrated torque. The relay asserts the TW32F output when the integrated torque, after a few tens of microseconds, exceeds a security margin.

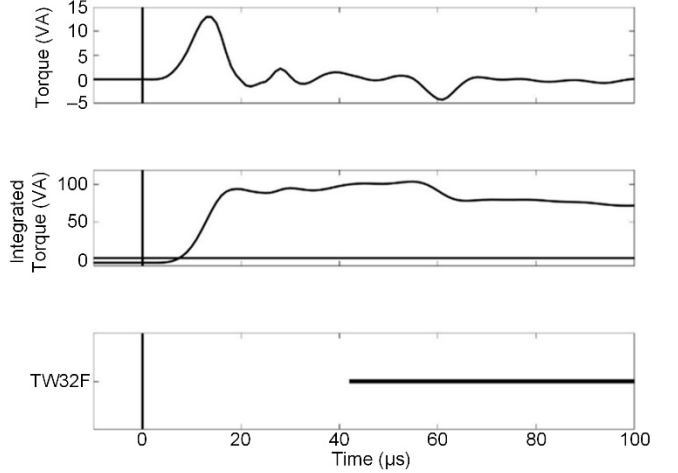


Fig. 15. Integrated torque is positive and exceeds the minimum required threshold to assert TW32F

Fig. 16 shows the current traveling waves from Terminal L and Terminal R associated with the faulted Phase A.

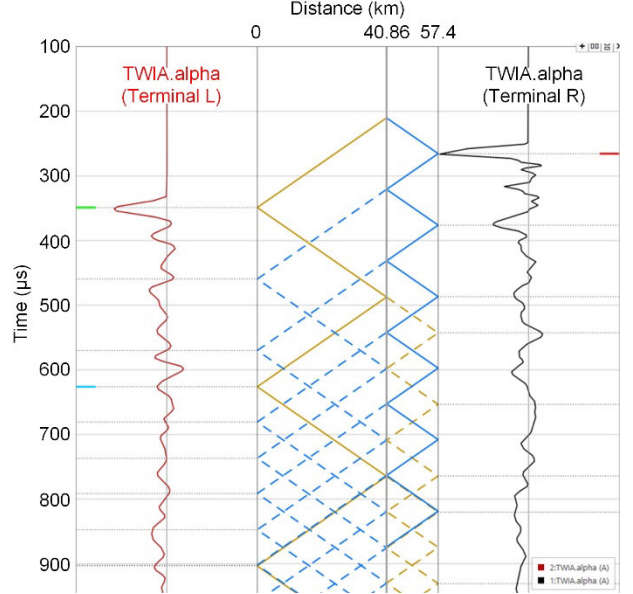


Fig. 16. Phase A current traveling waves and Bewley lattice diagram from Terminals L and R for the January 18, 2018 fault

Based on the first wave arrival times, the fault location from Terminal L was as shown in (5).

$$FL_L = \frac{57.4 \text{ km}}{2} \cdot \left( 1 + \frac{84.313 \mu\text{s}}{199.075 \mu\text{s}} \right) = 40.86 \text{ km} \quad (5)$$

### C. Phase-A-to-Ground Fault, January 20, 2018

Fig. 17 and Fig. 18 show the voltages and currents captured at Terminals L and R, respectively, for the third fault. The traveling-wave directional element (TW32) operated in 120  $\mu$ s, and the incremental-quantity directional (TD32) and distance (TD21) elements operated in 1.22 ms and 2.4 ms, respectively, at Terminal L. In this event, the fault was at 40 percent of the reach setting. Fig. 17 also shows the in-service phasor-based distance element operating time for comparison. The Zone 1 phasor-based distance element (Z1) operated in 18 ms.

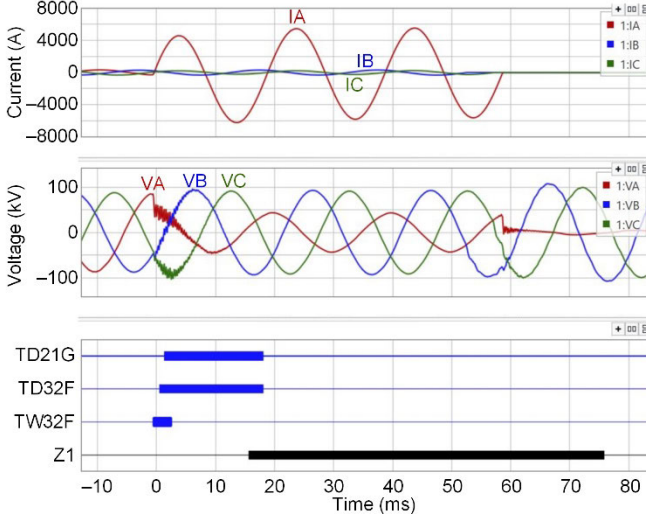


Fig. 17. Currents and voltages captured at Terminal L for the January 20, 2018 fault

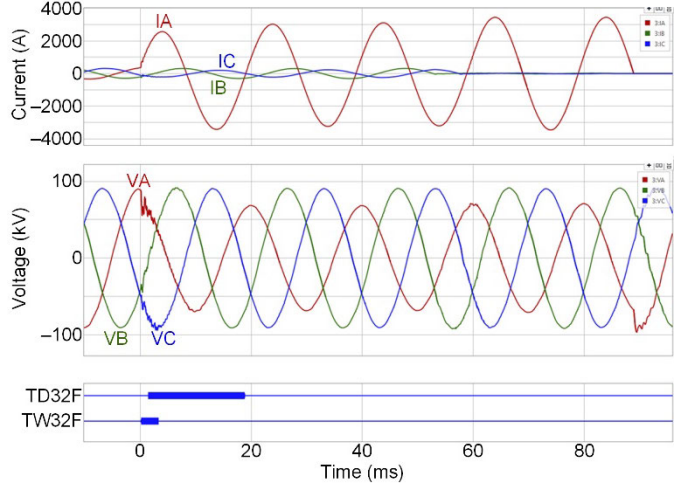


Fig. 18. Currents and voltages captured at Terminal R for the January 20, 2018 fault

Relays recorded two incipient fault events prior to this Phase-A-to-ground fault. The first incipient event happened at the negative peak of the voltage ( $t = 0$ ), the second event happened at the positive peak of the voltage ( $t = 10.29$  ms), and the Phase-A-to-ground fault happened at  $t = 10.74$  ms. Based on the timing associated with the current traveling waves from both terminals, the two incipient events and the fault occurred 14.06 km from Terminal L. Fig. 19 shows the phase current traveling waves from both terminals and the voltages from both terminals for the time span, including the two incipient fault events and the fault.

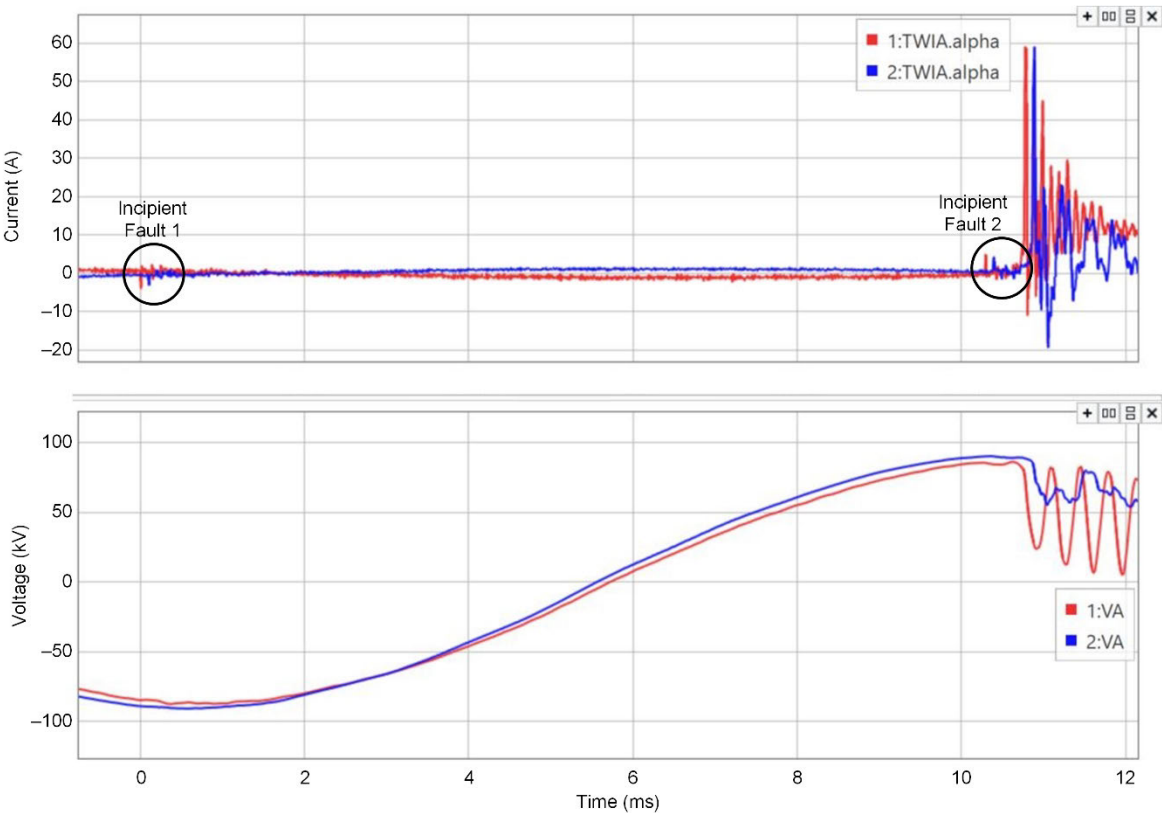


Fig. 19. Faulted phase current traveling waves recorded during the event

When the incipient fault or transient event is triggered at the negative voltage peak, a positive step change is injected into the line, resulting in a negative current traveling wave at the terminals (current polarity). With recording capability available to capture incipient faults, in the future, relays can detect and locate these faults and alarm the user if the number of incipient faults exceeds a threshold within a specific time window.

Fig. 20 shows the current traveling waves captured at Terminals L and R for the faulted Phase A.

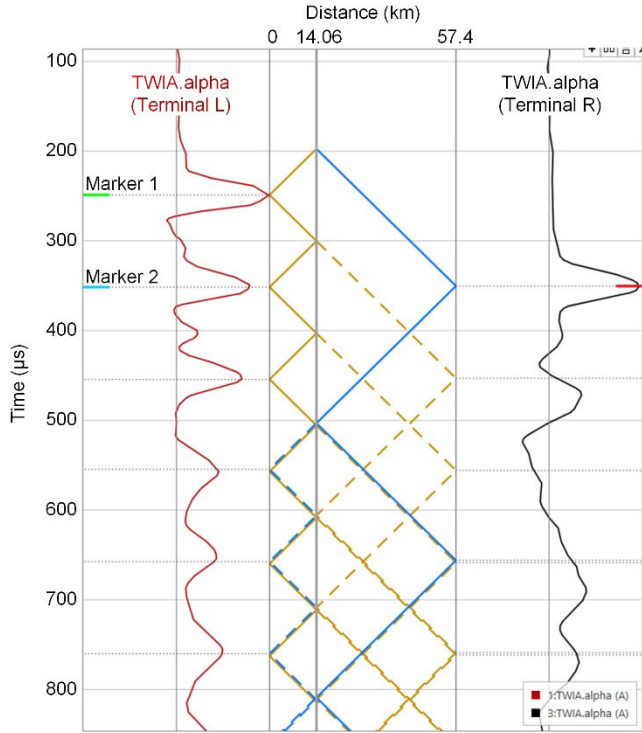


Fig. 20. Phase A current traveling waves and Bewley lattice diagram captured at Terminals L and R for the January 20, 2018 fault

Based on the first wave arrival times associated with the fault, the fault location from Terminal L was as shown in (6).

$$FL_L = \frac{57.4 \text{ km}}{2} \cdot \left( 1 - \frac{101.52 \mu\text{s}}{199.075 \mu\text{s}} \right) = 14.06 \text{ km} \quad (6)$$

Using only signals from Terminal L, the single-end TWFL method can be applied to calculate the fault location [9]. (Note that the single-end TWFL method can also be applied for the events discussed previously.) Using the time difference associated with Markers 1 and 2 in Fig. 20, the fault location is determined as shown in (7).

$$FL_{SE\_L} = \frac{57.4 \text{ km}}{2} \cdot \left( \frac{101.72 \mu\text{s}}{199.075 \mu\text{s}} \right) = 14.66 \text{ km} \quad (7)$$

## V. CONCLUSION

The utility where the pilot scheme is installed experienced challenges in locating faults on their power lines. They strongly believe that using technology to accurately locate faults and perform UHS fault clearing will improve their SAIDI and SAIFI indicators. This paper analyzed three internal faults on

the utility's system to demonstrate the performance of a line relay with TWFL and UHS protection functions.

Table II and Table III show the operating times of UHS protection functions at Terminal L and Terminal R, respectively. The directional elements operated in less than 3 ms, and the maximum operating time of the distance element is 10 ms.

TABLE II  
OPERATING TIMES OF PROTECTION FUNCTIONS AT TERMINAL L

Terminal L	TD32 (ms)	TW32 (ms)	TD21 (ms)
Event 1 (AG), 16.85 km	2	–	10
Event 2 (AG), 40.86 km	1.31	0.11	–
Event 3 (AG), 14.06 km	1.22	0.12	2.4

TABLE III  
OPERATING TIMES OF PROTECTION FUNCTIONS AT TERMINAL R

Terminal R	TD32 (ms)	TW32 (ms)	TD21 (ms)
Event 1 (AG), 40.55 km	1.6	0.15	–
Event 2 (AG), 16.54 km	1.24	0.042	2.54
Event 3 (AG), 43.34 km	1.42	0.12	–

Using megahertz sampling and data recording, the relay captured a circuit breaker restrike event and incipient faults. Detecting and locating incipient faults is an active area of research. The advanced recording capability in UHS relays allows detection of incipient faults, and it also opens the possibility of investigating potential issues in primary equipment.

## VI. REFERENCES

- [1] T. W. Stringfield, D. J. Marihart, and R. F. Stevens, "Fault Location Methods for Overhead Lines," *Transactions of the American Institute of Electrical Engineers – Part III: Power Apparatus and Systems*, Vol. 76, Issue 3, April 1957, pp. 518–529.
- [2] P. F. Gale, "Overhead Line Fault Location Based on Travelling Waves and GPS," proceedings of the Precise Measurements in Power Systems Conference, Arlington, VA, October 1993.
- [3] S. Marx, B. K. Johnson, A. Guzmán, V. Skendzic, and M. V. Mynam, "Traveling Wave Fault Location in Protection Relays: Design, Testing, and Results," proceedings of the 16th Annual Georgia Tech Fault and Disturbance Analysis Conference, Atlanta, GA, May 2013.
- [4] E. O. Schweitzer, III, A. Guzmán, M. V. Mynam, V. Skendzic, B. Kasztenny, and S. Marx, "Locating Faults by the Traveling Waves They Launch," proceedings of the 67th Annual Conference for Protective Relay Engineers, College Station, TX, March 2014.
- [5] E. O. Schweitzer, III, B. Kasztenny, A. Guzmán, V. Skendzic, and M. V. Mynam, "Speed of Line Protection – Can We Break Free of Phasor Limitations?," proceedings of the 68th Annual Conference for Protective Relay Engineers, College Station, TX, March 2015.
- [6] E. O. Schweitzer, III, B. Kasztenny, and M. V. Mynam, "Performance of Time-Domain Line Protection Elements on Real-World Faults," proceedings of the 69th Annual Conference for Protective Relay Engineers, College Station, TX, April 2016.

- [7] B. Kasztenny, A. Guzmán, N. Fischer, M. V. Mynam, and D. Taylor, "Practical Setting Considerations for Protective Relays That Use Incremental Quantities and Traveling Waves," proceedings of the 43rd Annual Western Protective Rely Conference, Spokane, WA, October 2016.
- [8] A. Guzmán, M. V. Mynam, V. Skendzic, J. L. Eternod, and R. M. Morales, "Directional Elements – How Fast Can They Be?," proceedings of the 44th Annual Western Protective Relay Conference, Spokane, WA, October 2017.
- [9] E. O. Schweitzer, III, A. Guzmán, M. Mynam, V. Skendzic, B. Kasztenny, C. Gallacher, and S. Marx, "Accurate Single-End Fault Location and Line-Length Estimation Using Traveling Waves," proceedings of the 13th International Conference on Developments in Power System Protection, Edinburgh, United Kingdom, March 2016.

## VII. BIOGRAPHIES

**Sthitaprajnya Sharma** received his post-graduate diploma in international business, with honors, from the Indian Institute of Foreign Trade in 2016, and he received his BE in electrical engineering, with honors, from Utkal University in 2006. He started his professional career with SPML as a power system design engineer. Later, he worked for ABB as a protection engineer. He joined Schweitzer Engineering Laboratories, Inc. in 2011 as an application engineer and is currently working as an application engineering manager in India. He has been involved in substation and generator protection, fast motor bus transfer solutions, application engineering, testing, and commissioning of protection and control solutions.

**Mangapathirao V. Mynam** received his MSEE from the University of Idaho in 2003 and his BE in electrical and electronics engineering from Andhra University College of Engineering, India, in 2000. He joined Schweitzer Engineering Laboratories, Inc. (SEL) in 2003 as an associate protection engineer in the engineering services division. He is presently working as a principal research engineer in SEL research and development. He was selected to participate in the U. S. National Academy of Engineering (NAE) 15th Annual U. S. Frontiers of Engineering Symposium. He is a senior member of IEEE and holds patents in the areas of power system protection, control, and fault location.